Geochemical Perspectives Letters

Moderately volatile element behaviour at high temperature determined from nuclear detonation

J.M.D. Day, F. Moynier, P.A. Sossi, K. Wang, A.P. Meshik, O.V. Pravdivtseva, D.R. Pettit

Supplementary Information

The Supplementary Information includes:

- The Trinity Test Site
- Figure S-1
- Detailed Methods
- Detailed Results
- Table S-1
- Supplementary Information References

The Trinity Test Site

The Trinity Test Site is in the Jornada Del Muerto desert region of New Mexico. At 5:29:45 am on the 16th July 1945, the world's first atomic nuclear detonation occurred at the 'zero point'. A ^{239}Pu implosion device (Y-1561, the 'Gadget') detonated at ~30 m height on a steel tower, with the equivalent force of 84 TJ, or ~21,000 metric tons of trinitrotoluene (TNT) (*e.g.*, Eby *et al.*, 2010). The geology in and around the region of the test site is dominated by quaternary sediments and cover. This arkosic desert sand is mineralogically complex, with alluvial, aeolian, evaporitic, and volcanic material (quartz, potassium feldspar, plagioclase, carbonates, sulfates, chlorides, detrital zircon, monazite, apatite, clay minerals and hornblende, olivine, magnetite, ilmenite and augite; Ross, 1948; Staritzky, 1950; Eby *et al.*, 2015). Additionally, the site was covered in manmade materials, including copper wires, the tower and casing (concrete) for 'the Gadget', and 'the Gadget' itself, which has led to heterogeneous compositions of resultant materials at the site (Eby, 2010; Fahey *et al.*, 2010; Bellucci *et al.*, 2014; Eby *et al.*, 2015).

The site experienced a range of conditions during the sequence of detonation of 'the Gadget' (Semcow *et al.*, 2006). Within three seconds of detonation, temperatures around the blast exceeded 8430 K (Hermes and Strickfaden, 2005). After 'bubble collapse', entrainment, vaporisation and melting of desert arkosic sand on the ground and within the mushroom cloud occurred, leading to a 'hot cloud condition' for 14 to 20 seconds. This condition was followed by ~8-11 seconds of 'freeze out' (Semkow *et al.*, 2006) and the fallout of a fused molten arkosic sand glass termed 'trinitite'. The fallout of trinitite at the rate of 0.36 cm s^{-1} (~1300 cm hr^{-1}) yielded a glass layer, on average, ~1 cm thick (Hermes and Strickfaden, 2005). The trinitite materials extended radially from zero point to ~370m (Storms, 1965). In detail, the dynamics of the detonation led to a heterogeneous distribution of trinitite glass across the site (Hermes and Strickfaden, 2005) (Fig. S-1) and to inhomogeneous glass being formed due to rapid heating and cooling (Eby *et al.*, 2010; 2015; Bellucci *et al.*, 2014).

The majority of trinitite is green in colour, although there is a sub-group of red coloured trinitite glasses. The glass has been described as falling, completely molten, with a fine sprinkling of dust. The glass is highly vesicular and similar to scoria (Eby *et al.*, 2010), with bubbles ranging from μm-size, to almost the complete diameter of the glass layer (~15 mm; Ross, 1948; Staritzky, 1950).

The presence of support structures, Pb bricks and Cu-rich wires used at the site for detonation and observation purposes, and material from 'the Gadget' itself, are thought to have led to the formation of metal in the trinitite, and the characteristic Cu-rich, red trinitite (Eby *et al.*, 2010; 2015). In general, the concentration of metal is greater in the red trinitite (2.7 to 4.6 modal %), compared with the green trinitite (0.1 to 0.3 modal %).

Temperature estimates for the explosion in the location of the trinitite vary, but all suggest temperatures above those anticipated for typical basaltic magmatic eruption temperatures (typically ≤1250 °C). Ross (1948) noted that some of the quartz in the green trinitite has been converted to silica glass, implying temperatures in excess of 1670 °C. In general, the trinitite glass is quite heterogeneous at small-scales (<1 mm) due to inefficient mixing and the distribution of precursor mineral phases (Bellucci *et al.*, 2014; Eby *et al.*, 2015). Eby *et al.* (2010; 2015) have also noted that only α-quartz remains as a mineral constituent of the glass, with all other minerals melting to form glass or metal. These authors concluded that local conditions in the vicinity of trinitite formation exceeded 1600 °C and 8 GPa. Using the estimates of Ross (1948), Staritzky (1950) estimated the energy to form the trinitite (3100 m^3, or ~ 7.5×10^9 g; Hermes and Strickfaden, 2005), and not including vaporized materials, equated to $(4.3 \pm 0.5) \times 10^{12}$ J. In general, the temperatures and reducing conditions involved in the Trinity nuclear test, combined with the arkosic sandstone composition at the test site, make a good - although not perfect - analogue for planet formation processes.

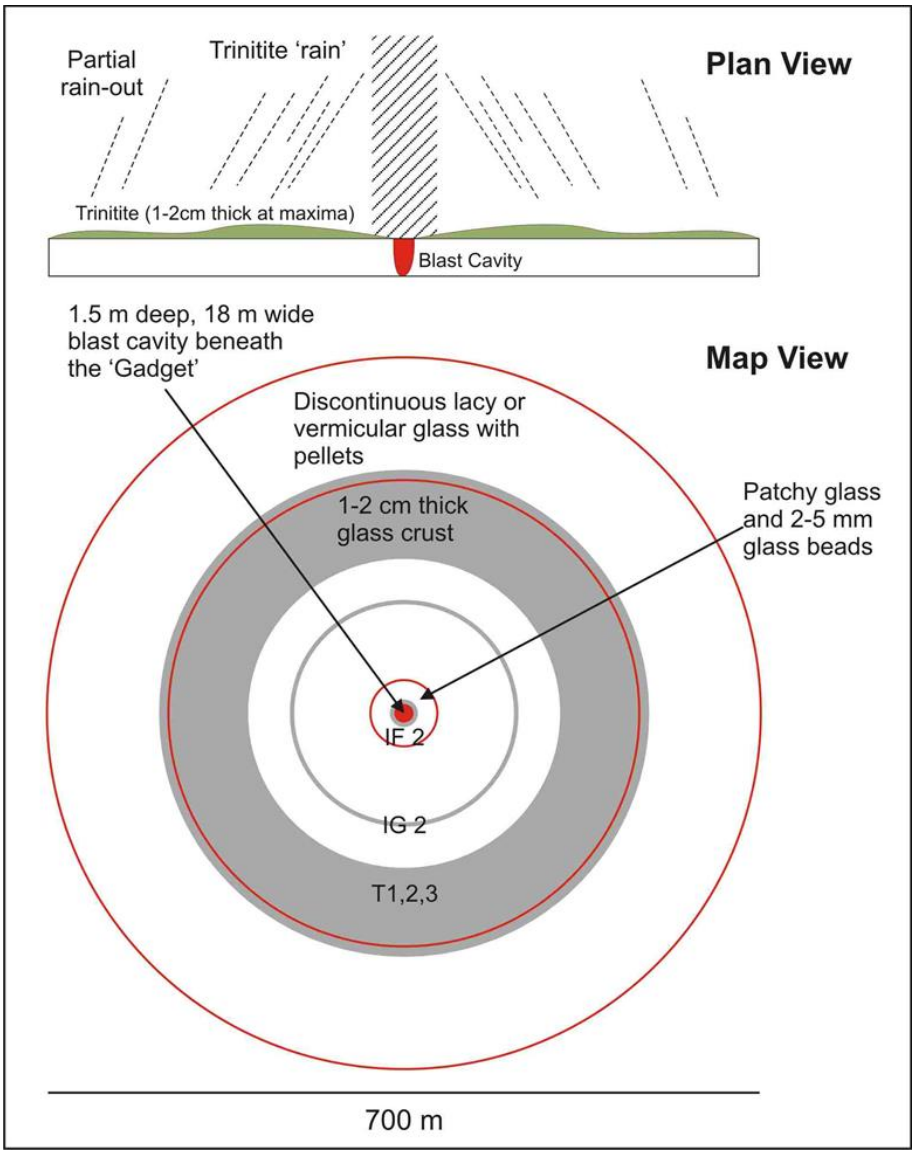

Figure S-1 Schematic of the 'geology' of trinitite at the Trinity Test Site, constructed from the observations of Ross (1948) and Staritzky (1950) and modified from Day *et al.* (2017). Grey bands show the locations of samples used in this study (shown as concentric rings).

Detailed Methods

A goal of studying the trinitite glasses was to assess Cu elemental or isotopic heterogeneity, and a systematic procedure of crushing and leaching/etching was designed and performed on samples at the Institut de Physique du Globe de Paris (Day *et al.*, 2017). Bulk powdered samples of IF, IG and T3 were analysed, with no leaching or modification. Powdered sample aliquots of IF and IG were leached and etched sequentially with 18.2 MΩ H_2O (20 min, ultra-sonification at 30 °C), 3 N HCl (20 min, ultra-sonification at 30 °C) and then with 1 N HF-HNO_3 (120 min, hotplate at 60 °C). After extraction of this final leaching stage, samples were dried down, and weighed prior to treatment in an identical fashion for dissolution, as described below. A total of eleven leachates/etchates, residues and whole-rock powders were measured for Cu isotope compositions and abundances.

After leaching/etching, all samples were dissolved in a 4:1 mixture of ultra-pure HF/HNO_3 in Teflon beakers for 96 hours, dried down and then dissolved and further dried down in 6M HCl twice to remove fluorides. In this study, remaining solutions, after Zn column chemistry (Day *et al.*, 2017), were used to obtain Cu isotope compositions. Samples and external standards were purified for Cu isotope analysis using a single column ion chromatographic technique (modified after Maréchal *et al.*, 1999). The procedure utilises Bio-Rad AG MP-1 anion resin, which, at low pH in chloride form, has a high partition coefficient for Cu. Sample aliquots were loaded onto the column and matrix elements were eluted in 8 ml of 7 N HCl. The Cu was then eluted in a further 22 ml of 7 N HCl. Samples were evaporated to dryness and the whole procedure was repeated to further purify Cu. The final Cu cuts, representing 99 ± 1 % of all Cu in the sample, were taken up in 0.1 N HNO_3 for analysis.

Copper isotope analysis was performed on a Thermo Fischer Neptune Plus Multi-Collector Inductively-Coupled-Plasma Mass-Spectrometer (MC-ICP-MS) at the Institut de Physique du Globe, Paris following similar procedures as in Savage et al. (2015) and Sossi et al. (2015). Samples were introduced into the instrument using an ESI PFA microflow nebuliser (100 µl min^{-1} flow rate) running into a quartz Scott double-pass spray chamber. The instrument was operated at low resolution (m/Δm ~ 450, where Δm is defined at 5 % and 95 % of peak height), with the ^{65}Cu and ^{63}Cu beams collected in the C (central) and L2 Faraday cups respectively. Matrix elements were monitored using ^{62}Ni and ^{64}Zn beams in L3 and L1 in the same cup set-up. Under typical running conditions, a 0.5 ppm Cu solution generated a 0.06-0.08 nA ion beam (6-8 V total signal using 10-11 Ω resistors). Instrument background signal (typically <10 mV total Cu) was measured at the beginning of each analytical session and the subsequent sample measurements were corrected for by using these data. The total procedural blank for the entire method contained ~4 ng Cu, which equates to between ~30% to <0.1% of the Cu analyte reported for samples in Table S-1. Consequently, all values are blank-corrected. Isotope ratios were measured in static mode, with each measurement consisting of 25 cycles of 8.4 second integrations, with a three second idle time. Ratios were calculated in the Thermo Neptune Data Evaluation software, which discarded any outliers at the 2-sigma confidence level. To correct for instrumental mass bias, isotope measurements were calculated using the standard sample bracketing protocol relative to the NIST SRM976 standard, whereby variations in Cu ratios are defined using the delta notation $\delta^{65}Cu$ as follows: $\delta^{65}Cu = [(^{65}Cu/^{63}Cu_{sample}/^{65}Cu/^{63}Cu_{SRM976}) - 1] \times 1000$. Analysis of two separate digestions of USGS standard reference material BHVO-2 gave $\delta^{65}Cu$ of 0.07 ±0.06‰ (2SD), in good agreement with the recommended literature value (0.12 ± 0.02 ‰, Moynier *et al.*, 2017).

Comparison of Cu contents measured by inductively coupled plasma mass spectrometry (ICP-MS; Day *et al.*, 2017) and column chemistry and MC-ICP-MS show that the ICP-MS measurements on ^{63}Cu give marginally higher total concentrations, likely due to minor interferences from $^{23}Na^{40}Ar+$ or $^{126}Xe^{++}$.

Detailed Results

Distal samples T1, T2 and T3 have between 49 and 73 µg g^{-1} Cu, with T3 having a $\delta^{65}Cu$ value of +0.10 ± 0.02 ‰ that is within the bulk silicate Earth (BSE) $\delta^{65}Cu$ estimate of +0.07 ± 0.10 ‰ (Savage *et al.*, 2015). Bulk sample IG (100 m) has a slightly lower Cu abundance (37 µg g^{-1}) and $\delta^{65}Cu$ of 0.40 ‰, and bulk sample IF (10 m) has low Cu (4.4 µg g^{-1}) and $\delta^{65}Cu$ of 0.30 ‰. Residues of IG and IF have lower Cu abundances (33 and 3.7 µg g^{-1}, respectively) and heavier $\delta^{65}Cu$ values (0.45 and 0.46 ‰) than bulk samples, whereas leachates yield higher concentrations of Cu and generally lighter $\delta^{65}Cu$ values (Table S-1). The exception to this relationship is the 3M HCl leach of IG which yielded a heavy $\delta^{65}Cu$ value (2.56‰). Recombination of residues etches and leaches of IG yield Cu contents and $\delta^{65}Cu$ (33.5 µg g^{-1}; $\delta^{65}Cu$ = 0.44 ‰) like the bulk sample. The same exercise for IF yields a slightly lower Cu content and heavier $\delta^{65}Cu$ value (4 µg g^{-1}; $\delta^{65}Cu$ = 0.44 ‰) than for the bulk sample.

Supplementary Table

Table S-1 Copper concentration and isotope data for trinitite glasses compared with Zn and K abundance and isotope data.

Sample	Distance (m)	Type	Mass (g)	Cu (μg g^{-1})	δ^{65}Cu	±2σ	Fraction	Blank%	∑Cu (μg g^{-1})	∑δ^{65}Cu	Cu (ICP)[a]	Zn (μg g^{-1})[a]	δ^{66}Zn[a]	K_2O (wt. %)[b]	δ^{41}K[b]
IF-2	10	Bulk	0.0386	4.4	0.30	0.04	100%	2.3%	4.4	0.30	7.39	13.2	0.72	3.3	-0.27
	10	Residue	0.3113	3.7	0.46	0.05	97%	0.3%	4.0	0.44		12.1	0.85		-0.27
		20m H_2O US	0.0004	25.3	-1.11	0.01	0.1%	30.5%				3.0			-0.41
		20m 3N HCl US	0.0012	18.6	-0.63	0.10	0.4%	14.8%				144.0	-0.09		-0.40
		2hr 1N HF-HNO_3	0.0065	11.8	-0.01	0.03	2.0%	4.9%				32.0	0.67		-0.26
IG-2	100	Bulk	0.0618	36.8	0.40	0.02	100%	0.2%	36.8	0.40	44.58	12.6	0.64	3.5	-0.45
	100	Residue	0.1966	32.8	0.45	0.04	96%	0.1%	33.0	0.43		10.2	0.65		-0.43
		20m H_2O US	0.0005	42.5	-0.07	0.12	0.2%	15.6%				17.6			-0.77
		20m 3N HCl US	0.0014	69.0	2.56	0.03	0.7%	3.8%				47.3	0.12		-0.34
		2hr 1N HF-HNO_3	0.0067	45.7	-0.23	0.01	3.3%	1.3%				31.0	0.63		-0.42
T-1	200	Bulk	0.0971								48.8	18.3		3.4	-0.48
T-2		Bulk	0.0911								58.1	17.4		3.6	-0.46
T-3	200	Bulk	0.1269	66.8	0.10	0.02		0.05%	66.8	0.10	72.8	16.3	0.31	3.51	-0.42

a - Copper and Zn concentrations and Zn isotopic data from Day *et al*. (2017); b - Potassium concentration and isotopic data from Chen *et al*. (2019).

Supplementary Information References

Chen, H., Meshik, A.P., Pravdivtseva, O.V., Day, J.M.D., Wang, K. (2019) Potassium isotope fractionation during the high-temperature evaporation determined from the Trinity nuclear test. *Chemical Geology* 522, 84-92.

Day, J.M.D., Moynier, F., Meshik, A.P., Pradivtseva, O.V., Petit, D.R. (2017) Evaporative fractionation of zinc during the first nuclear detonation. *Science Advances* 3, p.e1602668.

Eby, N., Hermes, R., Charnley, N., Smoliga, J.A. (2010) Trinitite – the atomic rock. *Geology Today* 26, 181-186.

Eby, G.N., Charnley, N., Pirrie, D., Hermes, R., Smoliga, J., Rollinson, G. (2015) Trinitite redux: mineralogy and petrology. *American Mineralogist* 100, 427-441.

Fahey, A.J., Zeissler, C.J., Newbury, D.E., Davis, J., Lindstrom, R.M. (2010) Post-detonation nuclear debris for attribution. *Proceedings of the National Academy of Sciences* 107, 20207-20212.

Hermes, R.E., Strickfaden, W.B. (2005) A new look at trinitite. *Nuclear Weapons Journal* 2, 2-7.

Maréchal, C.N., Télouk, P., Albarède, F. (1999) Precise analysis of copper and zinc isotopic compositions by plasma-source mass spectrometry. *Chemical Geology* 156, 251-273.

Moynier, F., Vance, D., Fujii, T., Savage, P. (2017) The isotope geochemistry of zinc and copper. *Reviews in Mineralogy and Geochemistry* 82, 543-600.

Ross, C.S. (1948) Optical properties of glass from Alamogordo, New Mexico. *American Mineralogist* 33, 360-362.

Savage, P.S., Moynier, F., Chen, H., Shofner, G., Siebert, J., Badro, J., Puchtel, I.S. (2015) Copper isotope evidence for large-scale sulphide fractionation during Earth's differentiation. *Geochemical Perspectives Letters* 1, doi: 10.7185/geochemlet.1506.

Semkow, T.M., Parekh, P.P., Haines, D.K. (2006) *ACS Symposium Series* 945, 142–159. American Chemical Society, Washington, D.C.

Sossi, P.A., Halverson, G.P., Nebel, O., Eggins, S.M. (2015) Combined separation of Cu, Fe and Zn from rock matrices and improved analytical protocols for stable isotope determination. *Geostandards and Geoanalytical Research* 39, 129-149.

Staritzky, E. (1950) Thermal effects of atomic bomb explosions on soils at Trinity and Eniwetok. *Los Alamos Scientific Laboratory*, LA-1126, 21pp.

Storms, B. (1965) Trinity. *Atom* 2, 1-34.